CHAPTER 2. ULTRA-WIDEBAND PHASE SHIFTER PRINCIPLES OF OPERATION

2.1. Introduction

A novel class of phase shifter is discussed and the principle of operation is explained. The unique frequency-independent quadrature property of symmetric couplers is shown to be the foundation of the success of these devices. The phase-shift characteristic is related to the coupling performance by a derived set of transform equations. The same freedom with respect to bandwidth and ripple is achieved as with the coupling properties. The phase shifter is compared to the tapered Tresselt phase shifter, and the practical bandwidth-limiting obstacles are shown to be eliminated.

2.2. Proposed Novel Ultra-wideband Phase Shifter

Shelton and Mosko realised that multisection parallel coupled TEM directional couplers and phase shifters are very closely related, and published a paper [1] on the synthesis and design of wideband equal ripple TEM directional couplers and fixed phase shifters. Both components were described as four-port networks, matched at all ports. In the directional coupler, a change in relative amplitude of the outputs with respect to the inputs is achieved, while in the phase shifter, a change in the relative phase of the outputs in comparison to the inputs is achieved.

Both the coupler and phase shifter were analysed, consisting of any number of equal $\lambda/4$ centre-frequency coupled sections. The analysis was based on inter-sectional reflections, all added at a reference plane, to derive the transfer amplitude or phase characteristic of the two components. It was found that the coupling characteristic of the device is the resultant of contributions of odd harmonics in θ. The electrical length of the coupled sections is proportional to frequency. For the phase shifter, the overall phase dispersion characteristic was found to be the result of contributions of even harmonics in θ. The analysis and design tables were all based on these foundations.

Had Shelton and Mosko [1] constructed their phase shifter with the end section half the length of all the other sections, they would have found the phase shifter and coupler response to be the result of contributions by odd harmonics in θ. Both components could then be analysed and designed equivalently, and a single set of design tables would have been sufficient. Two identical phase shifters can be joined in symmetry at the high-coupling ends, producing a symmetric coupler. A simple transform then relates the coupler and phase shifter performance parameters.

Shortly after the publication of Shelton and Mosko [1], Tresselt, the founder of the non-uniform line technique application to directional couplers, suggested applying the same techniques to this class of phase shifters [2]. As with the couplers, it was realised that the spread in coupling values between adjacent sections was large enough to produce significant reactive discontinuities in practical TEM line geometries, adversely affecting VSWR and phase accuracy of the device. Tresselt's paper [2] described the design of these phase shifters, which considerably alleviates the effect by employing coupling which is continuously tapered through the length of the device. A phase shifter was designed and constructed to be a continuously tapered device, starting with the prototype from tables provided by Shelton and Mosko. The layout of a typical Tresselt phase shifter is shown in Figure 6. The design equal ripple was from 1 GHz to 11.5 GHz, but measured results deviated at the high frequency end. It was concluded that the interconnecting strap at the end of the taper added parasitic components which could not sufficiently be compensated for beyond 9 GHz.

The problem was finally overcome by the novel coupler phase shifter proposed in this thesis. By using a hybrid coupler as vector processing element, symmetry can be introduced to avoid the interconnecting strap. The phase shifter response can be extended to 20 GHz and beyond. The layout of the novel phase shifter is shown in Figure 7. Standard coupler design tables such as published by Crystal and Young [3] can be used instead of special calculated phase shifter design tables.

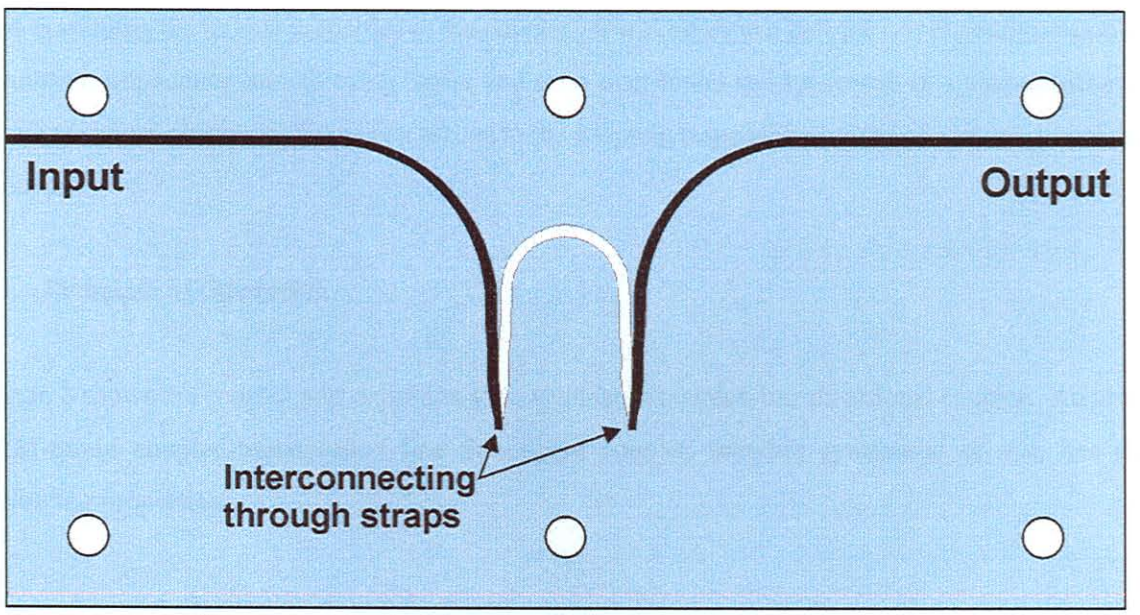

Figure 6 : Typical layout of Tresselt-based phase shifter

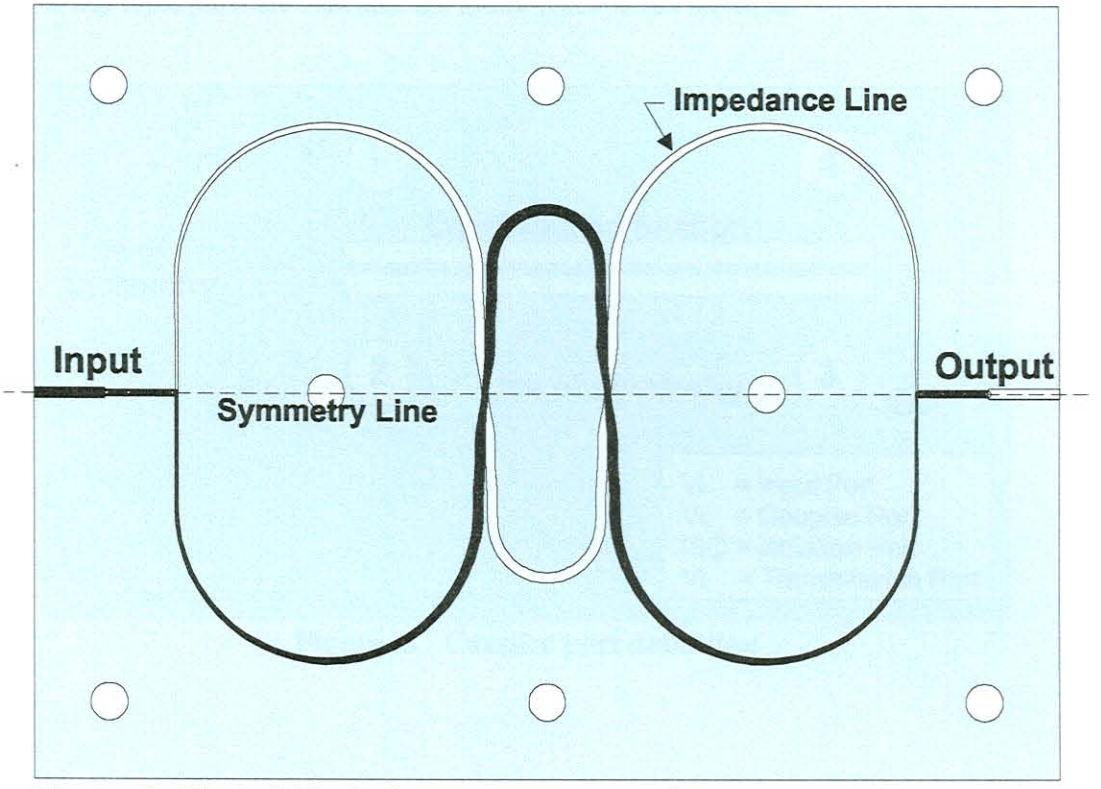

Figure 7 : Typical block diagram and layout of coupler-based phase shifter

The principle of operation of the proposed novel ultra-wideband phase shifter will be explained by first examining the unique properties of the coupler. It will be shown that the novel configuration of a coupler, impedance transforming tapers and semi-distributed splitters result in a phase shifter of which the phase characteristics can be related to the coupling response by means of a simple transform function.

2.3. Principle of Operation

Figure 8 shows the coupler port definition for a symmetric coupled-line directional coupler. An ideal TEM-mode coupled-transmission line directional coupler, whether symmetric or not, has the following properties:

- There is coupling of power from port 1 to port 2.
- There is transfer of power from port 1 to port 4.
- There is no transfer from port 1 to port 3 (isolation).

- If any three ports are matched, the fourth port appears matched.

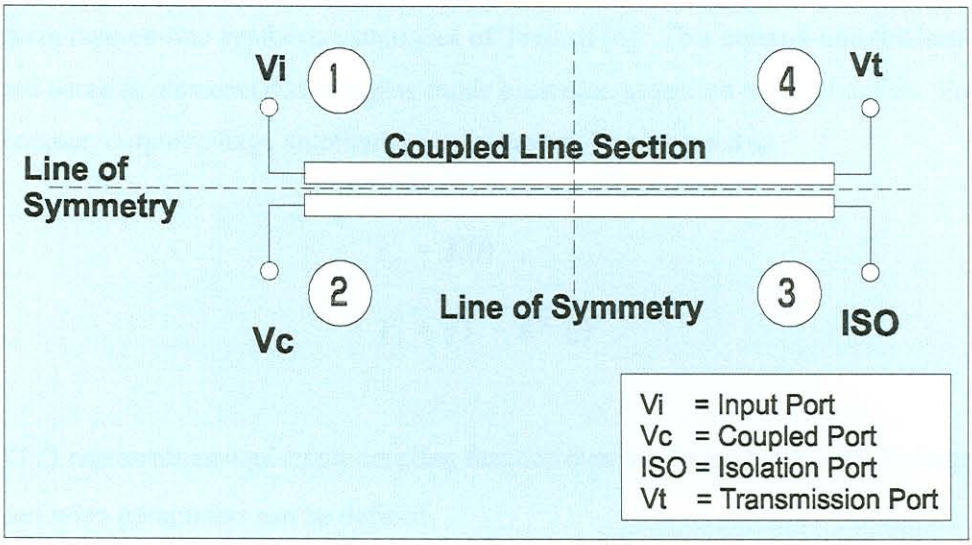

Figure 8 : Coupler port definition

Symmetric directional couplers have, in addition, the following unique and very valuable property:

- The coupled port (2) leads the transmission port (4) in quadrature at all frequencies [3, 4, 5].

This is the foundation on which the whole principle of operation is built. To fully understand the principle of operation of the phase shifter, it is necessary to review some relevant properties of symmetric directional couplers.

The coupling factor K of a coupler specifies the voltage ratio of coupled versus incident power . The coupling value (in decibel) can therefore be defined as

$$C = 20 \log (K) \quad . \tag{2.1}$$

A single section coupler only achieves this coupling coefficient over a limited band, depending on the ripple specification. However, by increasing the number of sections the bandwidth may be increased significantly. The number of sections and their coupling values depend on the bandwidth and ripple specification. Equal ripple Chebyshev multi-section coupler design tables, covering up to 20 : 1 bandwidth, have been tabulated by Crystal and Young [3].

Very high isolation and realisability into the mm-band can be achieved in stripline medium, using the non-uniform tapered-line synthesis techniques of Tresselt [4]. This tapered-line realisation avoids transitional parasitic elements due to higher mode excitation at section discontinuities. For a multi-section coupler, output voltage amplitudes can in general be expressed as

$$V_c = K(f) \quad , \tag{2.2}$$

$$V_t = \sqrt{1 - K^2(f)} \quad . \tag{2.3}$$

Where $K(f)$ represents an equi-ripple coupling function over the design bandwidth. Voltage coupling and transmission parameters can be defined

$$f_c = j e^{-j\theta} V_c \quad , \tag{2.4}$$

$$f_t = e^{-j\theta} V_t \quad . \tag{2.5}$$

Where the term $e^{-j\theta}$ accounts for the linear frequency dependant phase term caused by the physical length of the coupler. Examining the f_c and f_t functions, it is clear that f_c always leads f_t by 90°, independent of frequency. A coupler section is always a quarter wavelength long at the centre frequency. Symmetric couplers always have an odd number of sections. For a higher fractional bandwidth, more sections should be added to the coupler. As more sections are added to a wideband coupler of fixed lower cutoff frequency, the bandwidth and centre frequency are increased at roughly the same rate. As the centre frequency increases, the section lengths decrease. The physical length of a multi-sectional coupler therefore depends only on the lower cutoff frequency. The bandwidth and ripple (coupling deviation) is therefore fixed by the coupling nature of the device along its length.

For stripline couplers, the maximum achievable coupling over a broad band is practically about -6 dB. By connecting couplers in tandem, however, any coupling level can be achieved without compromising bandwidth or ripple. The electrical behaviour of a single ideal coupler as shown in Figure 9 may be described by an *S*-matrix

$$\begin{bmatrix} b_1 \\ b_2 \\ b_3 \\ b_4 \end{bmatrix} = \begin{bmatrix} 0 & f_c & 0 & f_t \\ f_c & 0 & f_t & 0 \\ 0 & f_t & 0 & f_c \\ f_t & 0 & f_c & 0 \end{bmatrix} \cdot \begin{bmatrix} a_1 \\ a_2 \\ a_3 \\ a_4 \end{bmatrix}, \tag{2.6}$$

where the f_c and f_t functions are as defined before in (2.4) and (2.5). The couplers discussed here may be single section narrow-band, or wideband tapered-line devices, in which case the coupling factors $K(f)$ in equations (2.2) and (2.3) become equi-ripple coupling functions. To interconnect the right ports of tandem connected couplers, it is necessary to cross the coupled lines as shown in Figure 9. From the figure it is also clear that the tightest coupling is in the middle of the coupler, and the slackest at the ends. Single section couplers, however, have the same coupling throughout the length of coupled lines such as shown in Figure 8.

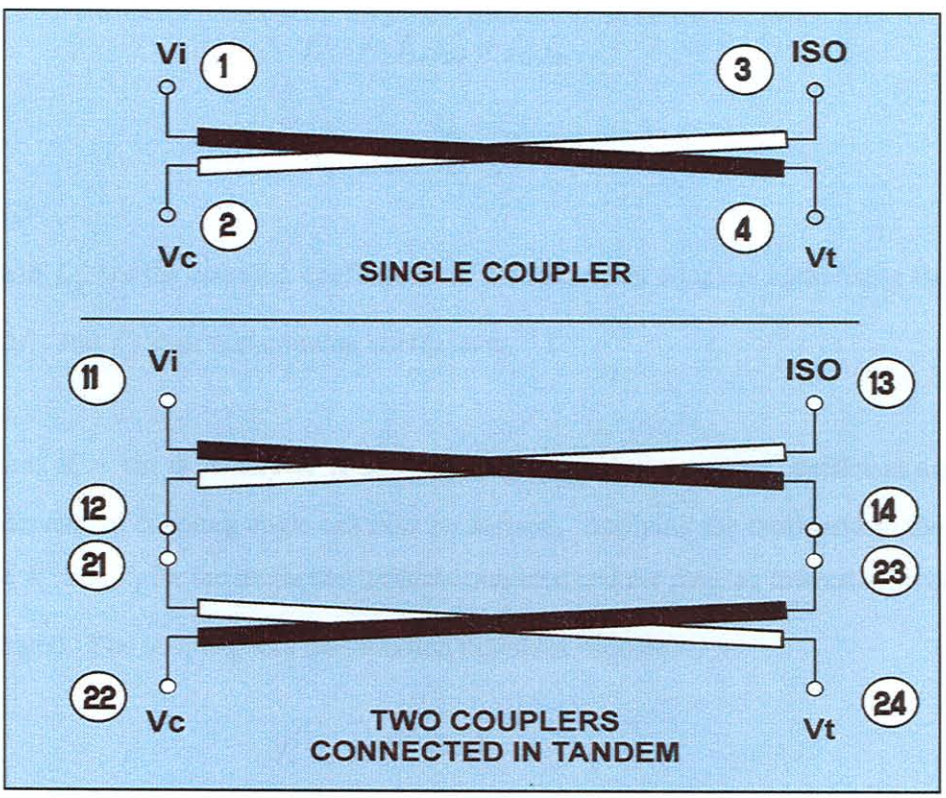

Figure 9 : Single and tandem connected couplers

Classical coupler theory can be presented in an alternative form to clarify the phase shifter principles. Let f_c' and f_t' represent the effective coupling and transmission coefficients of the tandem-connected coupler. Referring to Figure 9 it can be shown (Appendix A) that for the tandem-coupled case, the *S*-matrix becomes

$$\begin{bmatrix} b_{11} \\ b_{22} \\ b_{13} \\ b_{24} \end{bmatrix} = \begin{bmatrix} 0 & f_c' & 0 & f_t' \\ f_c' & 0 & f_t' & 0 \\ 0 & f_t' & 0 & f_c' \\ f_t' & 0 & f_c' & 0 \end{bmatrix} \cdot \begin{bmatrix} a_{11} \\ a_{22} \\ a_{13} \\ a_{24} \end{bmatrix} . \tag{2.7}$$

The tandem connected *S*-parameters f' can be written in terms of the separate coupler *S*-parameters f as

$$f_c' = f_{1c} f_{2c} + f_{1t} f_{2t} \ , \tag{2.8}$$

$$f_t' = f_{1c} f_{2t} + f_{1t} f_{2c} \ , \tag{2.9}$$

where f_{1c} and f_{2c} are the coupling coefficients of the individual couplers comprising the tandem coupler, and f_{1t} and f_{2t} their transmission coefficients.

The transform $K = \sin \phi$, where K is the frequency-dependent coupling coefficient and ϕ the frequency-dependent coupling angle can now be defined. Applying the transform to the original definition of V_c and V_t for the single and tandem-connected coupler case, an interesting concept can be demonstrated. The coupling and transmission functions become

$$f_c = j e^{-j\theta} \sin \phi \ , \tag{2.10}$$

$$f_t = e^{-j\theta} \cos \phi \ , \tag{2.11}$$

and for the tandem connected case in Figure 9, we find after substitution in equations (2.8) and (2.9) and simplifying,

$$f_c' = j e^{-j\theta} \sin(\phi_1 + \phi_2) \quad , \tag{2.12}$$

$$f_t' = e^{-j\theta} \cos(\phi_1 + \phi_2) \quad . \tag{2.13}$$

It can also be shown that, for n tandem-connected couplers of equal bandwidth,

$$f_{cn} = j e^{-j\theta} \sin(\phi_1 + \phi_2 + \ldots + \phi_n) \quad , \tag{2.14}$$

$$f_{tn} = e^{-j\theta} \cos(\phi_1 + \phi_2 + \ldots + \phi_n) \quad . \tag{2.15}$$

Therefore, adding equal-bandwidth couplers in tandem means adding their coupling angles. The compound coupling coefficient can then be calculated as follows: For couplers with individual coupling angles ϕ_1, ϕ_2 ... ϕ_n, the composite coupling angle with all connected in tandem, becomes

$$\phi_t = \phi_1 + \phi_2 \ldots + \phi_n \quad . \tag{2.16}$$

The resulting coupling coefficient becomes

$$K_t = \sin \phi_t \quad , \tag{2.17}$$

and the coupling decibel value is

$$C_t = 20 \log K_t \quad . \tag{2.18}$$

Another important result is that the coupling angle ripple, or tolerance, of identical tandem-connected couplers, can also be added. If, for two couplers to be connected in tandem,

$$\phi_1 = \phi_{01} \pm \delta\phi_1 \quad , \tag{2.19}$$

$$\phi_2 = \phi_{02} \pm \delta\phi_2 \quad . \tag{2.20}$$

Then the tandem connected couplers would yield a coupling angle of

$$\phi_t = (\phi_{01} + \phi_{02}) \pm (\delta\phi_1 + \delta\phi_2) \quad , \tag{2.21}$$

where ϕ_{01} and ϕ_{02} are the mean values, and $\delta\phi_1$ and $\delta\phi_2$ the ripple values of coupler 1 and coupler 2 respectively. Therefore, this forms a new coupler of added mean and ripple coupling angle values. The mean coupler angle and coupling coefficient can be related by the next equation:

$$C_0 = 20\log\left[\sin(\phi_0)\right] \quad . \tag{2.22}$$

The ripple-added values are defined by the following equation:

$$C_0 + \delta C = 20\log\left[\sin(\phi_0 + \delta\phi)\right] \quad . \tag{2.23}$$

and substituting equation (2.22) in (2.23), and solving for δC, yields

$$\delta C = 20\log\left[\frac{\sin(\phi_0 + \delta\phi)}{\sin(\phi_0)}\right] \quad . \tag{2.24}$$

It can also be demonstrated that by employing more couplers in tandem, the mean coupling value (C_0) and ripple specification (δC) of each individual coupler slackens, where C_0 and δC are the mean and ripple coupling values in dB, respectively. For n identical tandem-connected couplers, the resultant ripple coupling value is therefore

$$\delta C_n = 20\log\left[\frac{\sin(n\phi_0 + n\delta\phi)}{\sin(n\phi_0)}\right] \quad . \tag{2.25}$$

While the output phasors are always in perfect quadrature, their amplitude ratio depends on the coupling factor K. It follows directly from the principle of energy conservation that if one phasor amplitude increases, the other phasor amplitude will decrease. Therefore, the coupling ripple is amplitude- superimposed on these phasors and will be 180° out of phase, conserving input energy. These vectors are presented in Figure 10.

Realising this unique and important condition, phase shifters with ultra-wideband coverage can be synthesized [6,7]. A phase shifter is formed when the output voltages V_c and V_t of a coupler are vector-added and the result compared to the input of the coupler:

$$f_o = f_c + f_t \quad , \tag{2.26}$$

$$= e^{-j\theta}\cos\phi + j\, e^{-j\theta}\sin\phi \quad , \tag{2.27}$$

$$= 1\, e^{j\phi} e^{-j\theta} \quad . \tag{2.28}$$

Comparing the result to a reference line of electrical length θ, as is in the case of differential phase shifters, the term $e^{-j\theta}$ falls away. Therefore, if the output ports of a ϕ coupling-angle coupler are hard-wired, the output provides a vector with a phase shift ϕ relative to a reference line of same electrical length over the device bandwidth. The coupling angle ripple $\delta\phi$ becomes the phase shift ripple. To add phase shift ϕ^+, a coupler of coupling angle ϕ^+ must be added in tandem. By splitting the input signal and exciting both the input and isolated port with identical signals, a symmetric phase shifter evolves as shown in Figure 11. This improves high frequency operation due to the fact that the effect of small manufacturing errors tend to cancel in symmetric networks. This can be explained by the observation that errors generally occur in both phasors and do not contribute to phase shift errors of the combined result. This principle is demonstrated in APPENDIX B.

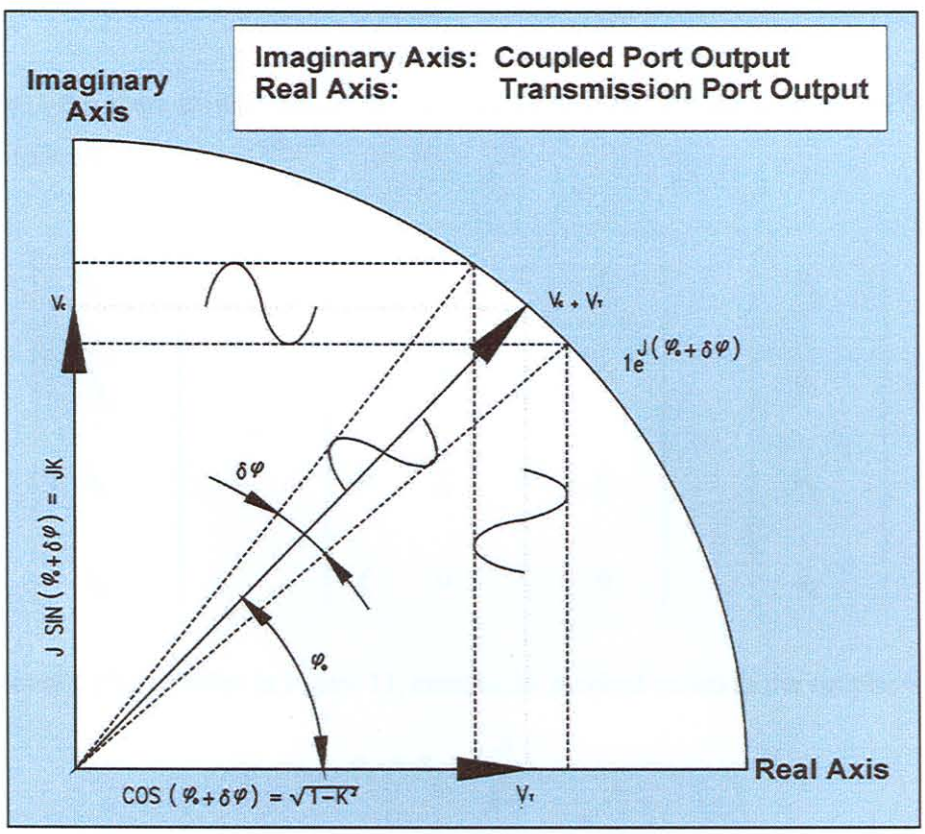

Figure 10 : Vector representation of coupler response

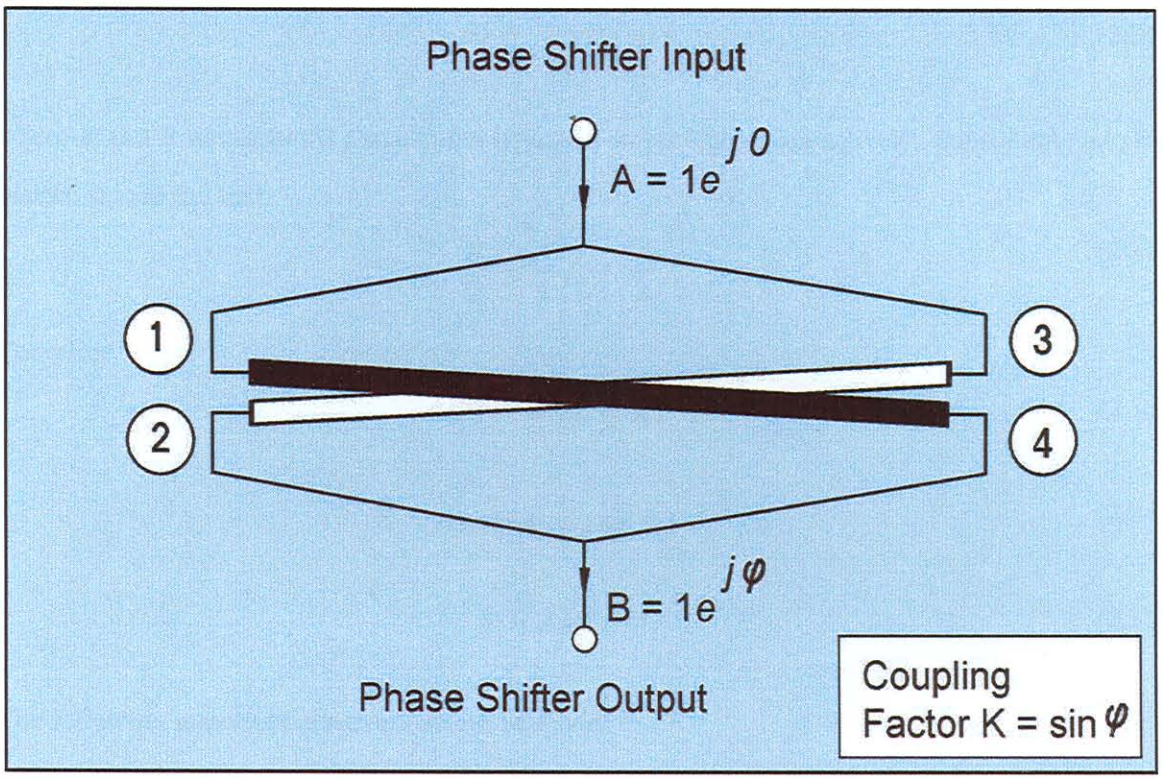

Figure 11 : Symmetric phase shifter

From Figure 11 the phase shifter transfer function can be derived. For the coupler, the *S*-parameter matrix is as follows:

$$\begin{bmatrix} b_1 \\ b_2 \\ b_3 \\ b_4 \end{bmatrix} = \begin{bmatrix} 0 & f_c & 0 & f_t \\ f_c & 0 & f_t & 0 \\ 0 & f_t & 0 & f_c \\ f_t & 0 & f_c & 0 \end{bmatrix} \cdot \begin{bmatrix} a_1 \\ a_2 \\ a_3 \\ a_4 \end{bmatrix} \qquad (2.29)$$

For the symmetric phase shifter in Figure 11, assume the incident waves to the coupler to be

$$a_1 = a_3 = \frac{A}{\sqrt{2}}, \qquad (2.30)$$

and the waves exiting the coupler to be

$$b_2 = b_4 = \frac{B}{\sqrt{2}} \quad , \tag{2.31}$$

where A and B represent the phase shifter input and output signals respectively. Substituting into the matrix, it is found that

$$\frac{B}{2} = \frac{A}{2} f_c + \frac{A}{2} f_t \quad . \tag{2.32}$$

Therefore

$$B = A(f_c + f_t) \quad , \tag{2.33}$$

$$B = A(\cos\phi + j\sin\phi)\, e^{-j\theta} \quad , \tag{2.34}$$

$$B = A e^{j\phi} e^{-j\theta} \quad . \tag{2.35}$$

The following important observations can be made:

- The circuit is throughout matched from point to point and operate reflection less.
- There is theoretically no energy loss, because $|B/A| = 1$.
- The frequency dependant term $e^{-j\theta}$ is balanced out by the reference line.
- The transfer function reflects a phase difference ϕ which is the coupling angle of the coupler.

Therefore, in principle, a lossless phase shifter with phase shift characteristics similar in shape and bandwidth to the coupling nature of the coupler has been constructed. The phase shift and coupling values can be related with a simple transform equation.

References

[1] J. P. Shelton and J. A. Mosko, "Synthesis and design of wide-band equal-ripple TEM directional couplers and fixed phase shifters", IEEE Trans Microwave Theory Tech., vol. MTT-14, no. 10, pp. 462-473, Oct. 1966.

[2] C. P. Tresselt, "Broadband tapered-line phase shift networks", IEEE Trans. Microwave Theory Tech., vol. MTT-16, pp. 51-52, Jan. 1968.

[3] E. G. Crystal and L. Young, "Theory and tables of optimum symmetric TEM-mode coupled-transmission-line directional couplers", IEEE Trans Microwave Theory Tech., vol. 13, no. 5, pp. 544-558, Sept. 1965.

[4] C. P. Tresselt, "The design and construction of broadband high-directivity, 90-degree couplers using non-uniform line techniques", IEEE Trans Microwave Theory Tech., vol. 14, no. 12, pp. 647-656, Dec. 1966.

[5] J. A. G.Malherbe,"Microwave transmission line couplers", Artech House, Norwood, 1988.

[6] F. V. Minnaar, J. C. Coetzee, and J. Joubert,"The analysis and synthesis of a novel ultra - wideband microwave differential phase shifter", in IEEE AP MTT - Symp., Pretoria, S.A., pp.138-433, Nov 1995.

[7] F. V. Minnaar, J. C. Coetzee, and J. Joubert,"A novel ultra - wideband microwave differential phase shifter," IEEE Trans. Microwave Theory Tech., vol. 45, pp.1249 - 1252, Aug 1997.